Available online at www.sciencedirect.com

ScienceDirect

Nuclear Physics A 935 (2015) 18–27

NUCLEAR PHYSICS A

www.elsevier.com/locate/nuclphysa

Role of the diagonal and off-diagonal continuum–continuum couplings in the breakup of ^{8}B and ^{19}C on ^{58}Ni and ^{208}Pb targets

B. Mukeru [a,*], M.L. Lekala [a], A.S. Denikin [b,c]

[a] *Department of Physics, University of South Africa, Pretoria, South Africa*
[b] *Dubna International University, Dubna, Moscow Region, Russia*
[c] *Joint Institute for Nuclear Research, Flerov Laboratory of Nuclear Reactions, Dubna, Moscow Region, Russia*

Received 12 November 2014; received in revised form 18 December 2014; accepted 22 December 2014

Available online 31 December 2014

Abstract

The role of the diagonal and off-diagonal continuum–continuum couplings on Coulomb + nuclear, Coulomb and nuclear breakup cross sections is investigated for the ^{8}B + ^{58}Ni, ^{8}B + ^{208}Pb and ^{19}C + ^{208}Pb at 29.3, 170.3 and 1273 MeV incident energies respectively. Qualitatively, we found that, the diagonal continuum–continuum couplings are responsible for the large reduction of the differential Coulomb + nuclear and nuclear differential breakup cross sections at backward angles. At forward angles, this reduction is due to the off-diagonal continuum–continuum couplings. In the absence of these couplings, the nuclear breakup is the more dominant process, while when they are included, the Coulomb breakup becomes dominant. This shows that, the nuclear breakup is more affected by the continuum–continuum couplings than its Coulomb counterpart. Quantitatively, we found that, the off-diagonal continuum–continuum couplings reduce by 13.39%, 12.71% and 11.11% the Coulomb + nuclear breakup cross sections for the ^{8}B + ^{58}Ni, ^{8}B + ^{208}Pb and ^{19}C + ^{208}Pb reactions, respectively.

Keywords: Integrated breakup cross sections; Continuum–continuum couplings; Differential breakup cross sections

* Corresponding author.
E-mail address: bmukeru@gmail.com (B. Mukeru).

http://dx.doi.org/10.1016/j.nuclphysa.2014.12.007

1. Introduction

Breakup reactions induced by halo projectiles exhibit, in general, strong continuum–continuum couplings (ccc), and have attracted intense attention in recent time [1–7]. In Refs. [1–4], the role of these couplings on the elastic scattering and breakup cross sections has been investigated for different reactions by means of the CDCC (continuum discretized coupled-channels) method [8–11]. The results obtained showed that, the inclusion of the ccc in the coupling matrix element, results in the reduction of the breakup cross sections. Similar studies were undertaken in Refs. [5–7] for the fusion cross sections, where it was also concluded that these couplings are responsible for the reduction of the fusion cross sections by increasing the Coulomb barrier. Particularly in Ref. [5], the authors showed that the ccc have a significant influence on the complete fusion cross section and it is also important to the total fusion cross section. However, most of these results were obtained by including in the coupling matrix element, either couplings to and from the ground state plus only diagonal couplings, or couplings to and from the ground state plus the ccc (both diagonal and off-diagonal couplings). It is therefore not clear how off-diagonal couplings affect the different reaction channels qualitatively and quantitatively, although in Ref. [6], it was mentioned that the role of off-diagonal couplings could be negligible on the fusion cross section. One could wonder how insignificant they are? It could be also important to know how they affect other reaction channels, like elastic breakup, which is part of the focus of this work.

The use of the CDCC method for such studies, considered in the aforementioned works and this work, is mostly justified by the fact that it includes accurately the ccc in the coupling matrix element. Moreover, both Coulomb and nuclear breakups are treated at the same footing [12]. However, due to the inclusion of the ccc (which may be strong) in the coupling matrix element, the method is computationally expensive. As a result, this method, although promising, has been limited to low and medium energy reactions [13]. From our experience, CDCC calculations converge faster when off-diagonal couplings are excluded than when they are included. It is therefore advantageous to have a clear idea on the role of off-diagonal couplings, as this could lead to an important simplification of the computational load.

The main goal of this paper, is to study the role of both diagonal and off-diagonal ccc on the Coulomb + nuclear, Coulomb and nuclear breakups as well as the Coulomb–nuclear interference for the ^{8}B + ^{58}Ni, ^{8}B + ^{208}Pb and ^{19}C + ^{208}Pb reactions at incident energies of 29.3 MeV, 170.3 MeV and 1273 MeV, respectively. The choice of these reactions is motivated, on one hand by the fact that there are elastic scattering data for the ^{8}B + ^{58}Ni, ^{8}B + ^{208}Pb reactions at these energies [14,15], which would guide our insight. On the other hand, there is an amount of theoretical works on these reactions, thus making the comparison easy. Moreover, the analysis of the ^{19}C + ^{208}Pb reaction is not fully complete as there exist contradicting results regarding the nuclear breakup contribution [16,17]. The analysis of the role of the ccc on both Coulomb and nuclear breakup cross sections, would shed more light in better understanding the dynamics of this reaction.

Throughout this paper, we shall use the following notations: nccc (no continuum–continuum couplings), dccc (diagonal continuum–continuum couplings), odccc (off-diagonal continuum–continuum couplings) and accc (all continuum–continuum couplings). For the sake of clarity, the symbol $\sigma_{\rm nccc}$ represents the breakup cross section resulting from couplings to and from the ground state only, $\sigma_{\rm dccc}$ cross section resulting from couplings to and from the ground state plus the dccc, and $\sigma_{\rm odccc}$ from couplings to and from the ground state plus the odccc, while $\sigma_{\rm accc}$ breakup cross section resulting from all the different couplings. To analyze the role of the odccc

Table 1
Optical model parameters for the nucleon–target used in the calculations. The parameters V_0, r_0, a_0 refer for to the depth, reduced radius and diffuseness of the real part, W_V, r_V, a_V stand for the volume imaginary part, while W_D, r_D, a_D correspond to the surface imaginary part. The reduced radii are converted to absolute radii as $R_x = r_x A_t^{1/3}$.

	V_0 (MeV)	r_0 (fm)	a_0 (fm)	W_V (MeV)	r_V (fm)	a_V (fm)	W_D (MeV)	r_D (fm)	a_D (fm)	r_C (fm)	Ref.
$p + {}^{58}$Ni	42.6	1.17	0.75	7.24	1.26	0.58	2.59	1.26	0.58	1.25	[20]
$p + {}^{208}$Pb	59.1	1.244	0.646	0.52	1.244	0.646	8.41	1.246	0.58	0.615	[21]
$n + {}^{208}$Pb	29.48	1.17	0.75	13.18	1.26	0.58	–	–	–	–	[16]

Table 2
Optical potential parameters for the core–target and CDCC input parameters. The different parameters are explained in Table 1. The reduced radii are converted to absolute radii as $R_x = r_x(A_c^{1/3} + A_t^{1/3})$.

	Core–target potential parameters							
	V_0 (MeV)	r_0 (fm)	a_0 (fm)	W (MeV)	r_W (fm)	a_W (fm)	r_C (fm)	Ref.
^{7}Be + ^{58}Ni	150.0	1.190	0.50	60.0	1.150	0.62	1.20	[20]
^{7}Be + ^{208}Pb	114.2	1.286	0.853	12.4	1.739	0.807	–	[22]
^{18}C + ^{208}Pb	200.0	0.631	0.9	76.2	0.77	0.58	–	[16]

on the different breakup cross sections, we will compare the dccc and accc results. Our calculations are performed using FRESCO codes [13]. The paper is organized as follows: In Section 2, we present our results and discussions and Section 3 summarizes our conclusions. The analytical expressions of the coupling potentials are given in Appendix A.

2. Results and discussions

The mathematical description of the CDCC method is available in the literature, for instance in Refs. [8–11,13]. Therefore, the details are not repeated in this work. In this section, we present and discuss our results. The starting point is the description of the relevant inputs to obtain the projectile's ground and continuum states. For the ^{8}B projectile, the spectrum is known to contain only one bound state, with $J^\pi = 2^+$ and a proton separation energy $S_p = 0.137$ MeV. This proton is in a $0p3/2$ orbit coupled to the $\frac{3}{2}^-$ ground state of the ^{7}Be [18]. The ${}^7\text{Be} + p$ potential, $V_{cv}(r)$ consists of both nuclear and Coulomb terms. The nuclear term contains a Woods–Saxon plus a spin–orbit coupling component, whose parameters are, $V_0 = 44.65$ MeV, $V_{SO} = 19.59$ MeV fm^2, $R_0 = R_{SO} = 2.391$ fm and $a_0 = a_{SO} = 0.52$ fm, taken from [18]. The Coulomb term is a point–sphere Coulomb potential of radius $R_C = 2.391$ fm. For the ^{19}C projectile, we adopt the ${}^{18}\text{C}(0^+) \otimes n(2s_{\frac{1}{2}^+})$ ground state configuration as suggested in Ref. [17]. The ${}^{18}\text{C} + n$ potential parameters are the same as those of ${}^{14}\text{C} + n$ system, taken from Ref. [19], where we only modify the depth of the central part to fit the ${}^{18}\text{C} + n$ experimental separation energy. These parameters are, $V_0 = 58.02$ MeV, $V_{SO} = 23.761$ MeV fm^2, $R_0 = R_{SO} = 2.651$ fm and $a_0 = a_{SO} = 0.6$ fm. The parameters of the real and imaginary parts of the projectile-target potentials are listed in Tables 1 and 2. The CDCC model space parameters, including the ones relevant to discretize both ^{8}B and ^{19}C continuums, are presented in Table 3. These parameters are chosen based on the convergence requirements.

Table 3
CDCC model space input parameters.

Reaction	$\ell_{\max}$ ($\hbar$)	$\varepsilon_{\max}$ (MeV)	$\lambda_{\max}$ (–)	$r_{\max}$ (fm)	$R_{\max}$ (fm)	$L_{\max}$ ($\hbar$)
$^{8}B + ^{58}Ni$	3	8	3	80	500	1000
$^{8}B + ^{208}Pb$	4	9	4	80	1000	10 000
$^{19}C + ^{208}Pb$	4	9	4	80	1000	10 000

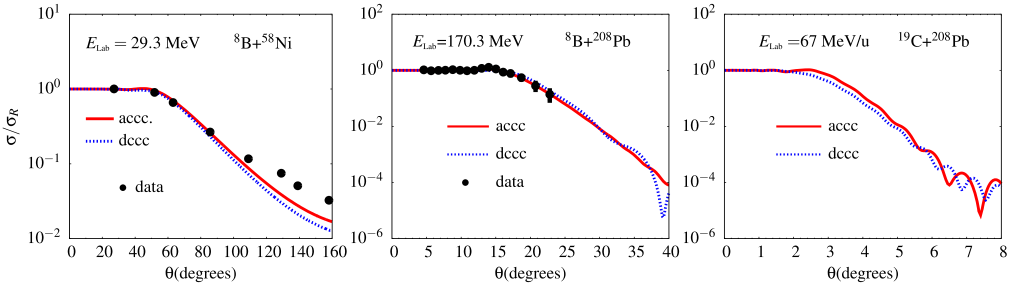

Fig. 1. $^{8}B + ^{58}Ni$, $^{8}B + ^{208}Pb$ and $^{19}C + ^{208}Pb$ elastic scattering cross sections. The data are taken from [14,15].

2.1. *Elastic scattering cross sections*

In Fig. 1, we present the results obtained for the elastic scattering cross sections, for the three reactions. The case where all the couplings are included (full curves), and the case where only the dccc (dotted curves) are included, are presented. A closer look at this figure shows that, for the $^{8}B + ^{58}Ni$ and $^{8}B + ^{208}Pb$ reactions, the effect of the ccc decreases as the charge of the target increases. Similar conclusions were drawn in Refs. [3,4] for the $^{8}B + ^{12}C$ and $^{8}B + ^{58}Ni$ reactions. For the $^{19}C + ^{208}Pb$, which is a neutron halo nucleus, the results reveal that, this effect is more pronounced than for the $^{8}B + ^{208}Pb$ reaction, and the tendency is to lower the cross section at angles between 2° and 5.5°.

2.2. *Differential breakup cross sections*

Here we discuss the angular distributions differential breakup cross sections for the $^{8}B + ^{58}Ni$, $^{8}B + ^{208}Pb$ and $^{19}C + ^{208}Pb$ reactions, respectively. The angular distributions differential breakup cross sections are presented in Figs. 2, 3 and 4 for the $^{8}B + ^{58}Ni$, $^{8}B + ^{208}Pb$ and $^{19}C + ^{208}Pb$ reactions, respectively. Let us first consider the $^{8}B + ^{58}Ni$ reaction, with the case where all the Coulomb and nuclear interactions are included coherently [see Fig. 2(a)]. The results show that the nccc breakup cross section is much extended to large angles, starting at the vicinity of the grazing angle ($\theta_{gr} \sim 50°$), and exhibits a minimum around 30°, similar to the results of [1,2]. On the other hand, when the dccc are included, the results show that this extension is completely removed, and the resulting breakup cross section drops rapidly, starting at the vicinity of the grazing angle, to become negligible beyond 100°. However, this breakup cross section is increased at forward angles ($10° \leq \theta \leq \theta_{gr}$). In the same figure we see that, including the odccc (that is to have all the ccc included), the corresponding breakup cross section (which is compared to the one obtained in the dccc case), increases at $\theta \geq 70°$ and decreases at $10° \leq \theta \leq 70°$. On the light of these results, it can be concluded that, the dramatic decrease of the Coulomb + nuclear breakup cross section beyond the grazing angle, is largely an effect of the dccc. On the other

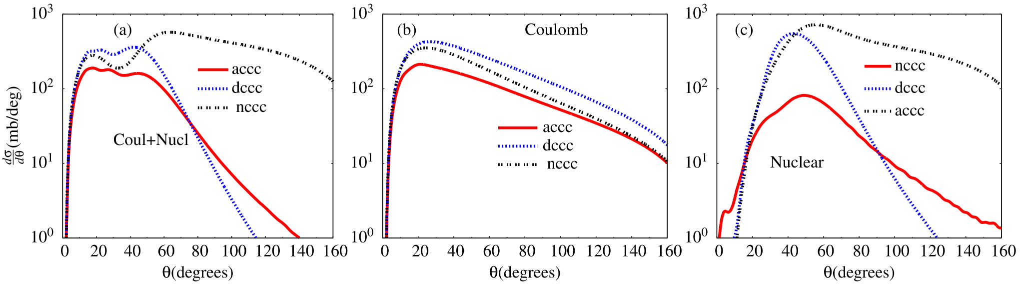

Fig. 2. Angular distribution cross sections for the ^{8}B + ^{58}Ni reaction.

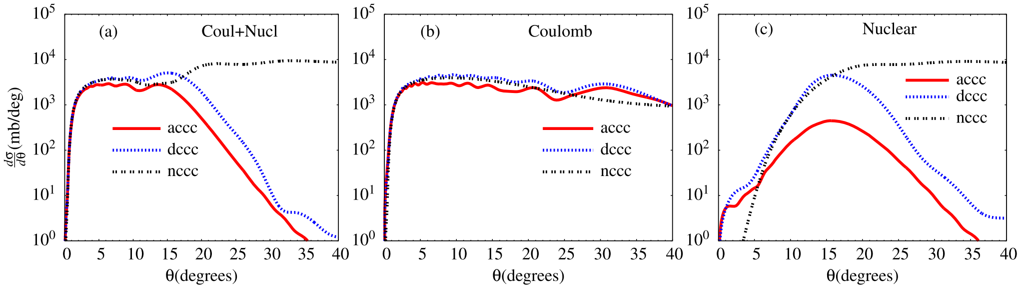

Fig. 3. Angular distribution cross sections for the ^{8}B + ^{208}Pb reaction.

hand, its decrease below the grazing angle, is an exclusive effect of the odccc. The reduction of the Coulomb + nuclear breakup cross section at large angles, is also reported in Ref. [3] for much lower incident energies.

The Coulomb breakup results presented in Fig. 2(b) (where the nuclear interactions are switched off), show that the inclusion of the dccc increases the breakup cross section at the whole range of angles starting from 10°. It can be seen that, the inclusion of the odccc decreases the breakup cross section, also starting from 10°, while their effect is similarly negligible beyond 100°. Lastly we consider, in Fig. 2(c), the ^{8}B + ^{58}Ni nuclear breakup, where it is clear that we can draw similar conclusions as in the Coulomb + nuclear case. However, at $\theta \leq 20°$, the effect of the dccc is negligible. Moreover, the inclusion of the odccc shows an increase of the breakup cross section at $\theta \leq 10°$. The results in Figs. 2(b) and (c) indicate that, the effect of the ccc on the Coulomb + nuclear breakup cross section is much dominated by the nuclear breakup.

We now turn to the ^{8}B + ^{208}Pb reaction, which involves a heavy target and an incident energy much higher than the Coulomb barrier. Our results are presented in Fig. 3. It is interesting to see that, the effect of the ccc show some similarities with the ^{8}B + ^{58}Ni reaction [see Fig. 2(a)]. However, here the odccc reduce the breakup cross section at the whole range of angles, starting from 5°. Concerning the Coulomb breakup [Fig. 3(b)], it can be seen that the ccc have small effect, in comparison with ^{8}B + ^{58}Ni reaction and the oscillatory pattern of the accc breakup cross section is due to the dccc. For the nuclear breakup however [Fig. 3(c)] the observation is that the dccc increase the nuclear breakup cross section at $\theta \leq 5°$, but results in its substantial reduction at $\theta \geq 15°$. The inclusion of the odccc, leads to a large decrease of the breakup cross section at $5° \leq \theta \leq 40°$.

To investigate whether one could obtain similar conclusions for a neutron halo nucleus, we repeated similar calculations for the ^{19}C + ^{208}Pb reaction. The results obtained are presented

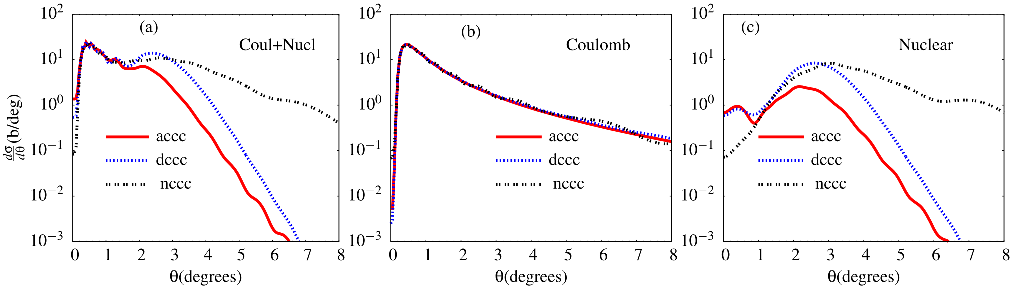

Fig. 4. Angular distribution cross sections for the ^{19}C + ^{208}Pb reaction.

Table 4
Integrated angular distributions cross sections in barns. The numerical integrations are performed up to $\theta_{max} = 180°$ for ^{8}B + ^{58}Ni, $\theta_{max} = 40°$ for ^{8}B + ^{208}Pb and $\theta_{max} = 8°$ for ^{19}C + ^{208}Pb.

Reaction	Coulomb + nuclear			Coulomb			Nuclear		
	σ^{C+N}_{nccc}	σ^{C+N}_{dccc}	σ^{C+N}_{accc}	σ^{Coul}_{nccc}	σ^{Coul}_{dccc}	σ^{Coul}_{accc}	σ^{Nucl}_{nccc}	σ^{Nucl}_{dccc}	σ^{Nucl}_{accc}
^{8}B + ^{58}Ni	54.106	17.143	9.900	21.040	28.378	14.042	52.814	17.087	3.870
^{8}B + ^{208}Pb	236.791	72.198	42.094	90.684	114.403	82.830	207.336	39.563	4.638
^{19}C + ^{208}Pb	378.211	224.216	111.971	113.660	112.162	108.308	277.429	123.381	32.859

in Fig. 4. In Fig. 4(a), the results obtained for the Coulomb + nuclear breakup case are shown, where again one observes that the resulting breakup cross section is much extended at large angles, starting as well at the vicinity of the grazing angle ($\theta_{gr} = 2.8°$). From the same angle, when the dccc are included, it is noticed, as in the previous case, that there is a substantial reduction of the breakup cross section which becomes negligible beyond 7°, although it is slightly increased at forward angles (between 1° and 2°). The inclusion of the odccc, results in a reduction of the breakup cross section at $1° \leq \theta \leq 7°$. We find that, the ccc have no effect on the Coulomb breakup cross section [see Fig. 4(b)], other than removing its oscillatory behavior. As for the nuclear breakup [Fig. 4(c)], similar conclusions as in the Coulomb + nuclear breakup case are reached, in line with the two other reactions. However, at $\theta \leq 10°$, the dccc increase the breakup cross section, where the inclusion of the odccc results in a negligible effect. The results as summarized in Figs. 2–4, show clearly that the Coulomb breakup cross section in the ^{19}C + ^{208}Pb reaction is much less affected by the cccc than in the other two reactions. However, these reactions present many similarities when regarding the effect of the ccc on breakup cross sections. In the vicinity of the grazing angles and beyond, the breakup cross section are largely reduced by the dccc, while below the grazing angles, they are reduced by the odccc.

2.3. *Integrated breakup cross sections and Coulomb–nuclear interference*

Qualitatively, we have seen in the above discussions that the odccc play an important role at small scattering angles. For a quantitative understanding of the effect of the ccc, we compute the integrated breakup cross sections for the three reactions under investigation. The results are presented in Table 4. As it can be seen, in the nccc case, the nuclear breakup is the more dominant process and the corresponding breakup cross sections amount to 71.51%, 69.57% and 70.94% of the incoherent integrated Coulomb + nuclear breakup cross sections for the ^{8}B + ^{58}Ni, ^{8}B + ^{208}Pb and ^{19}C + ^{208}Pb reactions, respectively. In the presence of all the ccc, it is seen that the

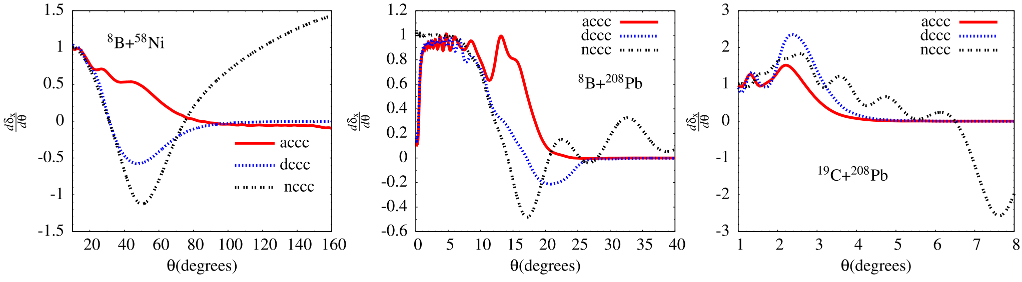

Fig. 5. Angular distributions of the ratios δ_x.

Coulomb breakup prevails, and the resulting breakup cross sections contribute respectively up to 78.39%, 94.70% and 76.72% of the incoherent Coulomb + nuclear breakup cross sections. This shows once again that, the nuclear breakup is the most affected by the ccc. Considering only the Coulomb + nuclear breakup, we find that, the ccc reduce 81.7% of the coherent breakup cross section for the ^{8}B + ^{58}Ni reaction, distributed as follows: 68.34% due to the dccc and 13.39% due to the odccc. For the ^{8}B + ^{208}Pb reaction, these couplings reduce the breakup cross section by 82.22%, where 69.51% is due to the dccc and 12.71% is due to the odccc. Similarly, for the ^{19}C + ^{208}Pb reaction, they reduce by 70.39%, with 59.28% being due to the dccc and 11.11% due to the odccc. Another remarkable aspect is that, the dccc increase the integrated Coulomb breakup cross section for the three reactions, although this increase is negligible for the ^{19}C + ^{208}Pb reaction. A careful look at this table shows that $\sigma_x^{C+N} - (\sigma_x^C + \sigma_x^N) < 0$, reflecting a destructive Coulomb–nuclear interference. Another way to analyze the nature of this interference is to use the ratio $\delta_x = (\sigma_x^{C+N} - \sigma_x^N)/\sigma_x^C$. In Ref. [23] (for $E_{cm} \leq 33$ MeV) it was also shown that this ratio is always less than one, corresponding to a destructive Coulomb–nuclear interference. Even at much lower energies ($E_{cm} \leq 9$ MeV), this interference was also found to be destructive [3]. To further get a clear understanding of the ccc effect on the Coulomb–nuclear interference (which is constructive, if $\delta_x \geq 1$), we present in Fig. 5, the angular distributions of δ_x ($\frac{d\delta_x}{d\theta}$). The results show that, for both ^{8}B + ^{58}Ni and ^{8}B + ^{208}Pb reactions, and in the nccc case, the Coulomb–nuclear interference is strongly destructive where the σ_{dccc} crosses the σ_{nccc} (i.e. in the vicinity of the grazing angles). This shows that, in the vicinity of the grazing angle, the nuclear breakup cross section is more important than the Coulomb + nuclear one. Also for the ^{8}B + ^{58}Ni reaction, one sees that the Coulomb–nuclear interference is exclusively constructive at $\theta \geq 80°$. This, among other reasons, is due to the fact that the Coulomb breakup cross section decreases significantly in this region. As for the ^{8}B + ^{208}Pb reaction, it is seen that at $\theta \geq 20°$, this interference is comparatively much less constructive, which is understandable given the importance of the Coulomb breakup cross section at these angles. Regarding the ^{19}C + ^{208}Pb reaction, on the other hand, this interference is mainly strongly destructive at large angles. Including the ccc, a substantial reduction of this interference is noticed. From the observations above, one concludes that the Coulomb–nuclear interference is strongly reduced by the ccc at large angles, and this is true for all the three reactions under consideration.

As already mentioned in the introduction, the reduction of the fusion cross section due to the ccc, results from the fact that these couplings increase the Coulomb barrier, and thus, lowering of the tunneling. To get more insight into how this affects the breakup cross sections, we determine the breakup cross sections inside the Coulomb barrier due the projectile flux that penetrates the barrier, and the breakup cross sections outside the barrier. To this end, we calculate the inte-

Table 5
Estimated Coulomb + nuclear, Coulomb and nuclear integrated breakup cross sections inside and outside the Coulomb barrier (in barns).

	$^{8}B + ^{58}Ni$ reaction								
	Coulomb + nuclear			Coulomb			Nuclear		
	nccc	dccc	accc	nccc	dccc	accc	nccc	dccc	accc
σ_{IB}	39.421	1.969	1.725	6.829	10.807	5.306	37.675	3.430	1.520
σ_{OB}	14.758	15.198	8.178	14.236	17.605	8.753	15.235	13.698	2.360
	$^{8}B + ^{208}Pb$ reaction								
	Coulomb + nuclear			Coulomb			Nuclear		
	nccc	dccc	accc	nccc	dccc	accc	nccc	dccc	accc
σ_{IB}	164.434	2.933	0.778	26.722	41.914	33.272	161.250	4.880	0.662
σ_{OB}	72.618	69.307	41.328	64.041	72.599	49.636	46.342	34.748	3.984
	$^{19}B + ^{208}Pb$ reaction								
	Coulomb + nuclear			Coulomb			Nuclear		
	nccc	dccc	accc	nccc	dccc	accc	nccc	dccc	accc
σ_{IB}	261.071	92.626	21.657	48.170	47.590	44.327	240.580	73.676	13.805
σ_{OB}	123.287	138.629	92.569	66.706	65.707	63.083	40.852	54.419	20.226

grated breakup cross sections inside (σ^{x}_{IB}) and outside (σ^{x}_{OB}) the Coulomb barrier, defined by the following expressions

$$\sigma^{x}_{IB} = \int_{\theta_{gr}}^{\theta_{max}} \frac{d\sigma_x}{d\theta} d\theta, \qquad \sigma^{x}_{OB} = \int_{0}^{\theta_{gr}} \frac{d\sigma_x}{d\theta} d\theta \tag{1}$$

The obtained results are presented in Table 5. It is clear from these results that, for the three reactions, the substantial reduction of the breakup cross sections inside the barrier is mainly due to the dccc, whereas the reduction outside the barrier is due to the odccc. It is seen that the odccc reductions are much weaker than the reductions due to the dccc, and thus resulting in larger nuclear breakup cross sections outside the barrier than inside.

3. Conclusions

We have investigated qualitatively and quantitatively the role of the ccc (both diagonal and off-diagonal couplings) on the Coulomb + nuclear, Coulomb and nuclear breakup cross sections for the $^{8}B + ^{58}Ni$, $^{8}B + ^{208}Pb$ and $^{19}C + ^{208}Pb$ reactions at different incident energies. To study the role of the odccc, we compared the results obtained when all the ccc are included, and the results obtained when only the dccc are included. Qualitatively, we found that, the dccc are largely responsible for the substantial reduction of the Coulomb + nuclear and nuclear breakup cross sections at large angles. At small angles, the reduction of these breakup cross sections, is due to the odccc. Regarding the Coulomb breakup, it is concluded that, for both $^{8}B + ^{58}Ni$, $^{8}B + ^{208}Pb$ reactions, the inclusion of the dccc give rise to an increase of the breakup cross section. However, for the $^{19}C + ^{208}Pb$ reaction, the effect of the ccc on the Coulomb breakup cross section was found to be rather negligible. Quantitatively, and considering only the Coulomb + nuclear breakup cross sections, we found that, the ccc reduce by 81.7% the coherent breakup cross section for the ^{8}B + ^{58}Ni reaction, distributed as follows: 68.34% due to the dccc and 13.39% due to the odccc. For the ^{8}B + ^{208}Pb reaction, on the other hand, these couplings reduce by 82.22%, where 69.51% is due to the dccc and 12.71% is due to the odccc, whereas for the ^{19}C + ^{208}Pb reaction, they reduce by 70.39%, where 59.28% is due to the dccc and 11.11% is due to the odccc.

In the absence of the ccc, the nuclear breakup is the more dominant process. The corresponding breakup cross sections contribute to the incoherent Coulomb + nuclear breakup cross section up to 71.51%, 69.57% and 70.94% for the three reactions ^{8}B + ^{58}Ni, ^{8}B + ^{208}Pb and ^{19}C + ^{208}Pb, respectively. The inclusion of all the ccc, favors the Coulomb breakup and the contributions of its breakup cross sections to the incoherent Coulomb + nuclear breakup cross sections, are in the following proportions 78.39%, 94.70% and 76.72% for the three respective reactions. This shows clearly that, the nuclear breakup is more affected by the ccc than its Coulomb counterpart. For the Coulomb–nuclear interference, our results showed that, this interference is strongly reduced by the ccc and mostly at large angles.

Appendix A. Coupling potentials

The continuum–continuum coupling (ccc) potentials are defined as

$$V^{LL'J}_{\alpha\alpha'}(R) = \langle \mathcal{Y}^{LJ}_{\alpha}(\mathbf{r}, \Omega_R) | U_{ct} + U_{vt} | \mathcal{Y}^{L'J}_{\alpha'}(\mathbf{r}, \Omega_R) \rangle, \tag{A.1}$$

where U_{ct} and U_{vt} are the core–target and nucleon–target phenomenological optical potentials, containing both Coulomb and nuclear components, and

$$\mathcal{Y}^{LJ}_{\alpha}(\mathbf{r}, \Omega_R) = \left[i^L \hat{\Phi}_{\alpha}(\mathbf{r}) \otimes Y_L(\Omega_R) \right]_{JM}. \tag{A.2}$$

In Eq. (A.2), the wave functions $\hat{\Phi}_{\alpha}(\mathbf{r})$ have the following expression

$$\hat{\Phi}_{\alpha}(\mathbf{r}) = \varphi_{\alpha}(r) \left[i^{\ell} Y_{\ell m_{\ell}}(\Omega_r) \otimes X_{s m_s} \right]_{jm}, \tag{A.3}$$

where $\varphi_{\alpha}(r)$ represents the bin wave functions defined as

$$\varphi_{\alpha}(r) = \frac{1}{\sqrt{W_{\alpha}}} \int_{k_{i-1}}^{k_i} \phi_{k\ell}(r) \mathrm{g}_{\alpha}(k) dk, \tag{A.4}$$

with $\phi_{k\ell}(r)$ being continuum wave functions of the projectile, normalized according to

$$\phi_{k\ell}(r \to \infty) \to F_{\ell}(kr) \cos\delta_{\ell j}(k) + G_{\ell}(kr) \sin\delta_{\ell j}(k), \tag{A.5}$$

in which F_{ℓ} and G_{ℓ} are Coulomb functions [13], and $\delta_{\ell j}(k)$ the nuclear phase shifts. W_{α} is some normalization coefficient and $\mathrm{g}_{\alpha}(k)$ is a function depending on the nature of the bin [13]. In Eq. (A.1), $V^{LL'J}_{\alpha\alpha'}(R)$ is separated into dccc (diagonal continuum–continuum couplings) $[V^{LL'J}_{\alpha=\alpha'}(R)]$ and odccc (off-diagonal continuum–continuum couplings) $[V^{LL'J}_{\alpha\neq\alpha'}(R)]$. The couplings to or from the ground state $[V^{LJ}_{\alpha\alpha_0}(R)$, $\alpha = (i, \ell, s, j)$, $\alpha_0 = (0, \ell, s, j)$, $i = 1, 2, 3, \ldots, N_b$, where N_b is the number of bins] are given by

$$V^{LJ}_{\alpha\alpha_0}(R) = \langle \mathcal{Y}^{LJ}_{\alpha}(\mathbf{r}, \Omega_R) | U_{ct} + U_{vt} | \mathcal{Y}^{LJ}_{\alpha_0}(\mathbf{r}, \Omega_R) \rangle. \tag{A.6}$$

Here the function $\mathcal{Y}^{LJ}_{\alpha_0}(\mathbf{r}, \Omega_R)$ is obtained by replacing in Eq. (A.3), the bin wave functions $\varphi_{\alpha}(r)$ with the projectile ground state wave function.

References

[1] F.M. Nunes, I.J. Thompson, Phys. Rev. C 57 (1998) R2818–R2820.
[2] F.M. Nunes, I.J. Thompson, Phys. Rev. C 59 (1999) 2652–2659.
[3] B. Paes, et al., Nucl. Phys. A 890 (2012) 1.
[4] J. Lubian, et al., Phys. Rev. C 79 (2009) 064605.
[5] A. Diaz-Torres, I.J. Thompson, Phys. Rev. C 65 (2002) 024606.
[6] A. Dias-Torres, I.J. Thompson, C. Beck, Phys. Rev. C 68 (2003) 044607.
[7] L.F. Canto, et al., Phys. Rev. C 80 (2009) 047601.
[8] Y. Iseri, et al., Prog. Theor. Phys. Suppl. 89 (1986) 84–117.
[9] E. Hiyama, Y. Kino, M. Kamimura, Prog. Part. Nucl. Phys. 51 (2003) 223–307.
[10] N. Austern, et al., Phys. Rev. C 53 (1996) 314–321.
[11] N. Austern, et al., Phys. Rev. Lett. 63 (1989) 2649–2652.
[12] N.C. Summers, F.M. Nunes, Phys. Rev. C 78 (2008) 011601R.
[13] I.J. Thompson, F.M. Nunes, Nuclear Reactions for Astrophysics, Cambridge University Press, New York, 2009.
[14] Aguilera, et al., Phys. Rev. C 79 (2009) 021601(R).
[15] Y.Y. Yang, et al., Phys. Rev. C 87 (2013) 044613.
[16] S. Typel, R. Shyam, Phys. Rev. C 64 (2001) 024605.
[17] T. Nakamura, et al., Phys. Rev. Lett. 83 (1999) 1112.
[18] G. Goldstein, P. Capel, D. Baye, Phys. Rev. C 76 (2007) 024608.
[19] P. Capel, H. Esbensen, F.M. Nunes, Phys. Rev. C 85 (2012) 044604.
[20] T.L. Belyaeva, et al., Phys. Rev. C 80 (2009) 064617.
[21] Y. Kucuk, A.M. Moro, Phys. Rev. C 86 (2012) 034601.
[22] S.J. Wang, et al., J. Phys. Conf. Ser. 420 (2013) 012075.
[23] Otomar, et al., Phys. Rev. C 87 (2013) 014615.